



Published in final edited form as:

Semin Thorac Cardiovasc Surg. 2022 ; 34(4): 1275–1284. doi:10.1053/j.semtcvs.2021.08.026.

Association of ongoing cerebral oxygen extraction during deep hypothermic circulatory arrest with post-operative brain injury

Jennifer M. Lynch, MD, PhD¹, Constantine D. Mavroudis, MD², Tiffany S. Ko, PhD³, Marin Jacobowitz, MSN³, David R. Busch, PhD⁴, Rui Xiao, PhD⁵, Susan C. Nicolson, MD⁶, Lisa M. Montenegro, MD⁶, J. William Gaynor, MD², Arjun G. Yodh, PhD⁷, Daniel J. Licht, MD³

¹The Children's Hospital of Philadelphia, Department of Anesthesiology and Critical Care Medicine, Philadelphia, Pennsylvania 19104

²The Children's Hospital of Philadelphia, Division of Cardiothoracic Surgery, Philadelphia, Pennsylvania 19104

³The Children's Hospital of Philadelphia, Division of Neurology, Philadelphia, Pennsylvania 19104

⁴Departments of Anesthesiology and Pain Management and Neurology, University of Texas Southwestern Medical Center, Dallas, Texas 75390

⁵University of Pennsylvania, Department of Biostatistics and Epidemiology, Philadelphia, Pennsylvania 19104

⁶The Children's Hospital of Philadelphia, Division of Cardiothoracic Anesthesia, Philadelphia, Pennsylvania 19104

⁷University of Pennsylvania, Department of Physics and Astronomy, Philadelphia, Pennsylvania 19104

Abstract

Objective: Cardiac surgery utilizing circulatory arrest is most commonly performed under deep hypothermia (~18°C) to suppress tissue oxygen demand and provide neuroprotection during operative circulatory arrest. Studies investigating the effects of deep hypothermic circulatory arrest (DHCA) on neurodevelopmental outcomes of patients with congenital heart disease give conflicting results. Here, we address these issues by quantifying changes in cerebral oxygen saturation, blood flow, and oxygen metabolism in neonates during DHCA and investigating the association of these changes with post-operative brain injury.

Methods: Neonates with critical congenital heart disease undergoing DHCA were recruited for continuous intraoperative monitoring of cerebral oxygen saturation (ScO₂) and an index of

Corresponding Author: Jennifer M. Lynch, The Children's Hospital of Philadelphia, 3401 Civic Center Blvd, Philadelphia, PA 19104, Phone: (215) 573-6406, lynchj3@email.chop.edu.

Declaration of conflicting interest:

Arjun G. Yodh has his name on four patents submitted on behalf of the Trustees of the University of Pennsylvania related to this work: US20190000321, US10064554, US20140343384, US8082015 but does not generate income.

Publisher's Disclaimer: This is a PDF file of an unedited manuscript that has been accepted for publication. As a service to our customers we are providing this early version of the manuscript. The manuscript will undergo copyediting, typesetting, and review of the resulting proof before it is published in its final form. Please note that during the production process errors may be discovered which could affect the content, and all legal disclaimers that apply to the journal pertain.

cerebral blood flow (CBF_i) using two non-invasive optical techniques, diffuse optical spectroscopy (DOS) and diffuse correlation spectroscopy (DCS). Pre- and post-operative brain magnetic resonance imaging (MRI) was performed to detect white matter injury (WMI).

Results: Fifteen neonates were studied, and 11/15 underwent brain MRI. During DHCA, ScO₂ decreased exponentially in time with a median decay rate of -0.04 min^{-1} . This decay rate was highly variable between subjects. Subjects who had larger decreases in ScO₂ during DHCA were more likely to have post-operative WMI ($p=0.02$).

Conclusions: Cerebral oxygen extraction persists during DHCA and varies widely from patient-to-patient. Patients with a higher degree of oxygen extraction during DHCA were more likely to show new WMI in post-operative MRI. These findings suggest cerebral oxygen extraction should be monitored during DHCA to identify patients at risk for hypoxic-ischemic injury, and that current commercial cerebral oximeters may underestimate cerebral oxygen extraction.

Keywords

congenital heart disease; deep hypothermic circulatory arrest; cerebral oxygen extraction fraction; cerebral oxygen metabolism; white matter injury; neonate; cerebral oxygen saturation

Introduction

Congenital heart defects (CHD) are the most common birth defect, affecting approximately 40,000 newborns each year in the United States. Nearly one third of these children require cardiac surgery during the neonatal period.¹ While surgical advances over the last several decades have improved survival, neurodevelopmental disabilities remain a significant morbidity among survivors. As a result, clinical and investigative focus has shifted from survival beyond the neonatal period toward neurologic sequelae. Magnetic resonance imaging studies during the neonatal period in this population exhibit a high prevalence of a specific form of hypoxic-ischemic white matter injury (WMI), which is identical in location and MRI characteristics to the punctate injury seen in premature infants termed periventricular leukomalacia.^{2,3} Notably, WMI in preterm survivors has been directly linked to long-term cognitive outcomes.⁴ Investigations of school age survivors who had various forms of CHD reveal problems with academic achievement, fine and gross motor function, visual-spatial skills, and executive function,^{5,6} all of which are similar to cognitive outcomes seen in survivors of prematurity.^{7,8}

Recent investigations have focused on identifying perioperative risk factors for WMI in CHD and subsequent neurodevelopmental disabilities. Although the exact timing and cause of perioperative WMI remains unknown, previous studies have identified cardiac diagnosis, brain immaturity, duration of deep hypothermic circulatory arrest (DHCA), and timing of surgery as risk factors.⁹⁻¹² Specifically, in a heterogeneous cohort of 153 infants with severe CHD, Beca et al. showed that risk for new or worsened postoperative WMI was highest in neonates with single ventricle physiology and was associated with brain maturity and with use and duration of DHCA.¹⁰ Other studies have not found an association between DHCA duration and WMI,^{11,13} and other techniques such as antegrade cerebral perfusion have not been shown to be superior to DHCA for neuroprotection.¹⁴

Overall, the published results are in conflict about the significance of DHCA on the risk of postoperative WMI. Thus, in this contribution we investigate changes in cerebral hemodynamics during DHCA and explore their association with WMI. We utilize non-invasive diffuse optical and diffuse correlation spectroscopies (DOS and DCS, respectively) to quantify cerebral oxygen saturation and blood flow continuously throughout the procedure.^{15–17} Specifically we investigate these changes during DHCA to ascertain whether deep hypothermia at ~18°C suppresses cerebral metabolism sufficiently to provide neuroprotection during circulatory arrest and how intraoperative cerebral hemodynamics relate to the risk for postoperative WMI.

Materials and Methods

Patient Population

The subjects reported herein were taken from a larger study cohort. All term newborns (37–42 weeks gestation) with pre- or post-natally diagnosed critical CHD admitted to the cardiac intensive care unit (CICU) at The Children's Hospital of Philadelphia (CHOP) were screened for study inclusion. Exclusion criteria included: birth weight less than 2 kg, a history of perinatal depression (i.e., 5-minute APGAR<5 or cord blood pH<7.0), perinatal seizures, evidence of end-organ injury, pre-operative cardiac arrest, and significant pre-operative intracerebral hemorrhage (e.g., grade 3 or 4 intraventricular hemorrhage). Since we were not studying neurodevelopmental outcomes, genetic syndromes were not an exclusion. Parents were approached for consent after birth and prior to day of surgery for pre- and post-operative MRI and optical monitoring during the perioperative period. A subset of enrolled patients who underwent cardiac surgery requiring DHCA is included in this manuscript.

Study Protocol

This study protocol has been described previously.^{11,16,18,19} All procedures were approved by the Institutional Review Board. Patient demographic data were recorded. On the morning of surgery, all patients received general anesthesia. Subsequently, they underwent a brain MRI for pre-operative injury assessment. After the MRI, a non-invasive optical probe was secured to the forehead for continuous DOS/DCS measurements of cerebral oxygenation (ScO₂), oxygen extraction fraction (OEF), and cerebral blood flow (CBF). In a subset of patients, a commercial oximeter (Nonin, SenSmart Model X-100) was also secured to the forehead for continuous monitoring of relative cerebral oxygen saturation (rSO₂). All patients underwent cardiac surgery utilizing cardiopulmonary bypass with DHCA. Antegrade cerebral perfusion was not used. pH-stat blood gas management was used during cooling and while hypothermic; alpha stat was used during rewarming and at normothermia per institutional protocol. Patients were cooled to a target nasopharyngeal (NP) temperature of 18°C prior to initiating DHCA.

Approximately 1 week after surgery, patients underwent a post-operative follow-up MRI scan without general anesthesia. This scan enabled us to assess the development and/or progression of brain injury.

DOS/DCS Measurements

Diffuse optical spectroscopy (DOS) and diffuse correlation spectroscopy (DCS) utilize near-infrared light to noninvasively probe static and dynamic physiological properties of cortical brain tissue. Our custom-made optical instrument combines these two techniques on a mobile cart that can be used in the operating room (Video 1).^{16,19,20}

DOS (also called frequency-domain near-infrared spectroscopy (FD-NIRS)) is a widely accepted method to quantify tissue oxygenation. Multi-distance frequency-domain DOS (FD-DOS), employed in this study, is capable of accurate quantification of cerebral tissue oxygen saturation (ScO_2), *i.e.*, in contrast to, commercial oximeters that employ continuous-wave NIRS (CW-NIRS) to monitor trends in cerebral oxygen saturation. FD-DOS uses photon diffusion theory to relate the measured amplitude attenuation and phase shift of modulated and multiply scattered light detected on the tissue surface to determine the wavelength-dependent tissue absorption (μ_a) and scattering (μ_s) properties. These properties are determined by fitting to the semi-infinite medium solution of the photon diffusion equation for a homogeneous medium. The phase and AC amplitude (AC) of the detected light quantify the optical properties of the tissue. Specifically, the slope of the phase versus source-detector separation on the tissue surface (r) and the slope of the $\ln(\text{AC} \times r^2)$ versus r were determined and used to compute μ_a and μ_s , respectively.¹⁵ Data were discarded if these linear fits had a Pearson correlation coefficient $R^2 < 0.975$, which was usually caused by probe dislodgement during patient repositioning.

The wavelength- and time-dependent absorption coefficient, $\mu_a(\lambda, t)$, in turn, depends linearly on oxy- ($[\text{HbO}_2]$) and deoxy-hemoglobin ($[\text{Hb}]$) concentration. Therefore, measurements of the tissue absorption at multiple wavelengths yield these two concentrations in absolute units. From $[\text{HbO}_2]$ and $[\text{Hb}]$, we derive total hemoglobin concentration ($\text{THC}=[\text{HbO}_2]+[\text{Hb}]$) and cerebral tissue oxygen saturation ($\text{ScO}_2=[\text{HbO}_2]/\text{THC}$). Cerebral oxygen extraction fraction (OEF) is calculated from ScO_2 and the arterial oxygen saturation (SaO_2) measured clinically from an arterial blood gas.¹⁹ Cerebral blood volume (CBV, mL/100g of tissue) can be calculated from THC.²¹ The FD-DOS device employed in the present study (Imagent, ISS Inc., Champaign, IL) is amplitude modulated at 110 MHz and employs source lasers at 2 wavelengths, $\lambda=688$ and 830 nm.

DCS uses near-infrared light to non-invasively monitor cerebral blood flow (CBF). DCS measures the temporal fluctuations (the temporal autocorrelation function) of the light intensity at the tissue surface which is primarily caused by moving red blood cells.^{15,22,23} The correlation diffusion equation and its semi-infinite solutions are employed to convert these temporal fluctuations into an index of cerebral blood flow (CBF_i , measured in units of cm^2/s).¹⁵ Although this index does not have traditional physiological units of CBF, recent studies have shown that CBF_i can be calibrated in absolute units, and that it correlates strongly with other gold standard measures of CBF.^{16,24–27} Jain et al., for example, validated this optically measured CBF_i against CBF measured in the superior sagittal sinus with phase contrast MRI in a similar population of infants with critical CHD.¹⁶

Importantly, the DCS-measured CBF_i can be combined with FD-DOS-measured ScO_2 and information about clinical arterial oxygenation measured from arterial blood samples to

derive an index of the cerebral metabolic rate of oxygen consumption ($CMRO_{2,i}$).^{19,20} Then a temperature coefficient, Q_{10} , can be calculated to assess the temperature-dependence of metabolism during the cooling period prior to DHCA.²⁸ Q_{10} is defined as the relative change in cerebral metabolic rate of oxygen per 10°C change in temperature:²⁸

$$Q_{10} = \left(\frac{CMRO_{2,1}}{CMRO_{2,2}} \right)^{\frac{10}{T_1 - T_2}} \quad (1)$$

The patient interface for this hybrid FD-DOS/DCS instrument consisted of a custom-made flexible black rubber probe secured to the subject's forehead with a soft wrap. The probe houses fiber optics for both FD-DOS and DCS. For FD-DOS, we used 4 source-detector separations (1.5, 2.0, 2.5, and 3.0 cm along the tissue surface), with 2 source fibers (*i.e.*, one for each wavelength at each separation) and 1 detection fiber. For DCS, 8 single-mode detection fibers were bundled and placed on the tissue surface 2.5 cm away from the source fiber.

Results

From July 2015 to April 2017, a total of N=32 neonates with complex CHD were recruited, and 27 of 32 underwent surgery requiring DHCA. Of these 27 subjects, n=15 had adequate optical data quality for further analysis (see Methods). Cardiac diagnoses for these 15 subjects include: hypoplastic left heart syndrome (n=9) and hypoplastic or interrupted aortic arch (n=6). Postoperative MRI scans were not acquired for 2 patients: 1 patient was deemed medically too unstable for postoperative MRI during study period and 1 subject was withdrawn from postoperative MRI by parental request. Additionally, MRI scans were not usable for 2 patients due to motion artifacts. Therefore, MRI data was available for 11 out of the remaining 15 subjects.

Patient demographics and operative parameters are summarized in Table 1. All patients were full term with an average gestational age of 38.6 ± 0.7 weeks. Patients waited an average of 3.7 ± 1.4 days from birth until their procedure. The median (IQR) duration of DHCA was 40 (12.8) minutes. Two subjects underwent a second run of bypass and one of these two subjects required DHCA during their second bypass run.

Figure 1 (top) shows continuous FD-DOS and DCS measurements throughout surgery for one patient. These data demonstrate typical changes that occurred during the monitoring protocol. The concentration of cerebral oxy-hemoglobin ($[HbO_2]$), and cerebral oxygen saturation (ScO_2), increases after the initiation of CPB, representing a decrease in cerebral oxygen extraction fraction while the patient's temperature is decreased to 18°C. ScO_2 decreases after the initiation of circulatory arrest. The cerebral blood flow index (CBF_i) falls dramatically to zero upon initiation of circulatory arrest and increases upon reperfusion. Similar trends are observed for all 15 subjects. Figure 1 (bottom) exhibits summary changes in ScO_2 and CBF_i for all 15 patients at different time points during surgery.

ScO₂ decreased during DHCA in all subjects, and the magnitude of this decrease was highly variable between subjects.

Figure 2 shows the trend of ScO₂ during DHCA for all 15 subjects. The average time on DHCA in this cohort was 41 minutes. ScO₂ decreases during DHCA for all subjects. Fitting ScO₂ versus time to an exponential decay model:

$$ScO_2 = ae^{-bt} \quad (2)$$

where t is time in minutes, yields an average initial value of 60.1 ± 13.5 and a median [IQR] decay constant of -0.04 [$-0.06, -0.01$]. A more negative decay constant trended toward increased risk for new WMI, but this was not statistically significant ($p=0.11$).

The presence and volume of WMI on pre- and post-operative MRI is summarized in Table 2. Optically measured changes in cerebral oxygenation predicted post-operative WMI. Specifically, larger decreases in ScO₂ during DHCA predicted presence of new WMI on postoperative MRI (Figure 3, $p=0.02$ from Wilcoxon rank-sum test, area under the receiver operating characteristic curve is 0.929 with 95% CI of 0.762–1.00).

This decrease in ScO₂ was not detected using commercially available cerebral oximetry. For the subset ($n=3$) of subjects wherein a commercial oximeter was also used, rSO₂ was compared with FD-DOS measured ScO₂ (Figure 4). Correlation between these two modalities was lost during DHCA, with the commercial oximeter consistently reporting an rSO₂ that was greater than FD-DOS measured ScO₂. In this small sample, the commercial oximeter underestimated the decrease of cerebral oxygen saturation during DHCA.

To investigate changes in oxygen metabolism with cooling, a quantitative index of cerebral metabolic rate of oxygen (CMRO_{2,i}) was obtained during the cooling period.

Figure 5 demonstrates the dependence of CMRO_{2,i} on nasopharyngeal temperature (NPT). This data yielded an average CMRO_{2,i} temperature coefficient Q_{10} of 1.5 ± 0.4 . Q_{10} , along with the duration of cooling prior to DHCA and the lowest nasopharyngeal temperature reached during the cooling period, did not predict the degree of metabolism suppression during DHCA, as defined by the change in ScO₂ during DHCA ($\Delta ScO_{2,DHCA}$) (Figure 6).

Discussion

This study reports the first use of diffuse optical and correlation spectroscopies for *continuous* monitoring of cerebral oxygen saturation, blood flow, and oxygen metabolism during DHCA in neonates. In all 15 subjects, ScO₂ decreased significantly during DHCA, signifying persistent oxygen extraction at 18°C, and the magnitude of this decrease in ScO₂ predicted the incidence of new post-operative WMI (Figure 7). To our knowledge, this direct association between continued cerebral oxygen requirement during DHCA and post-operative brain injury has not been previously shown; however, previous studies have suggested that brain metabolism persists at 18°C.^{29–31}

Beca et al. previously reported that DHCA was positively associated with severity of post-operative WMI.¹⁰ In the present study, duration of DHCA was not significantly different between subjects with or without new postoperative WMI. Other studies, including one from our group, also did not find a significant association between duration of DHCA and post-operative WMI.^{11,13} This difference in findings could be due to differences in the study population (*e.g.*, DHCA used for indications other than aortic arch repair), differences in criteria for defining WMI on MRI, institutional differences in operative protocols (*e.g.*, duration of cooling, DHCA and rewarming), or inclusion (or lack thereof) of possible cofounders in the prediction models. For example, we previously reported that the most significant risk factor for new post-operative WMI in a homogeneous population of infants with HLHS was time-to-surgery.¹¹ In the present study, a larger decrease in ScO₂ during DHCA, signifying greater oxygen extraction, correlated with new postoperative WMI. Since the present study was limited in the number of subjects with both useable optical data (*e.g.*, due to probe dislodgement after placement, see Methods) and postoperative MRI data, robust statistical multivariate analyses to investigate risk for new postoperative WMI could not be performed. Most likely, risk for postoperative WMI is multifactorial, and our small sample size limits the power of discovery for all but the most significant risks. For example, since time-to-surgery has been shown to correlate with lower preoperative ScO₂ on day of surgery and a higher risk of postoperative WMI,^{11,32} it is possible that a lower baseline ScO₂ could augment the effect of longer DHCA duration. Clearly, the relationship between ScO₂ during DHCA and postoperative injury warrants further investigation. One subject also underwent two runs of DHCA, and this subject also had a large amount of new WMI on post-operative MRI. However, even when removing this subject from analysis, subjects with new post-operative WMI still had a significantly greater decrease in ScO₂ during DHCA ($p=0.04$).

Furthermore, we observed a range of temporal decay curves/rates for ScO₂ during deep hypothermia (Figure 2). This variability demonstrates value for individual monitoring during DHCA, for example to determine an acceptable duration of circulatory arrest. Previous studies have also reported a range of acceptable durations for DHCA. Greeley et al. investigated the effect of deep hypothermia on cerebral oxygen metabolism and reported that cerebral metabolism decreased during deep hypothermia and neuroprotection was offered in the range of 39 to 65 minutes.³⁰ Similarly, Ko et al. reported a range of trends in CMRO₂ with temperature in neonatal swine.²⁸ Additionally in that study, nasopharyngeal temperature was shown to be an inaccurate surrogate marker for CMRO₂ based on the difference in the relationship between CMRO₂ and nasopharyngeal temperature during cooling versus rewarming. The findings in that study further speak to the importance of individualized cerebral oxygen metabolism monitoring intraoperatively during DHCA.

The temperature coefficient, Q₁₀, computed in this study ($Q_{10} = 1.5 \pm 0.4$) is lower than values reported in literature. Greeley et al. reported an average Q₁₀ of 3.35 [2.72, 4.17] in neonates and children, although there was a large variation in Q₁₀ values reported in that study and no attempt to separate the effect of age was made.³⁰ It is possible that this difference in temperature coefficients is due to the different methods used for calculating Q₁₀. Greeley et al. calculated CMRO₂ from CBF measured episodically by xenon-clearance methods and the arteriovenous oxygen content difference with venous blood sampled from

right jugular bulb. These measurements were performed at five discrete time points during cardiac surgery, and Q_{10} was calculated from the difference between two time points.³⁰ For the temperature coefficient reported herein, $CMRO_{2,i}$ was measured continuously, and the trend between $CMRO_2$ and NPT was fit to an exponential model to compute Q_{10} (see Ko et al.²⁸). The lower temperature coefficient measured during cooling reported here may also explain the continued cerebral oxygen extraction observed during DHCA; however Q_{10} was not correlated with $ScO_{2,DHCA}$ (Figure 6). Further studies with a larger cohort are needed to explore possible reasons for this difference in temperature coefficients, including anesthetic technique and cooling duration.

Interestingly, the decrease in ScO_2 captured by the commercial oximeter was not as substantial nor prolonged as the decrease captured by the more sophisticated and accurate FD-DOS device (Figure 4). In all 3 cases when both devices were utilized, the commercial oximeter yielded a plateau in ScO_2 of around 50% while ScO_2 quantified by FD-DOS continued to decrease. While believed to be accurate during normal conditions for monitoring trends, commercial oximeters likely fail, even for trend monitoring, during low blood volume states. The current generation of commercial cerebral oximetry devices do not have the ability to measure the concentration of hemoglobin in the sampled tissues as is possible with FD-DOS. In the near-infrared, the absorption of water and oxygenated hemoglobin follow the same broad trend of increased absorption with longer wavelengths, while absorption from deoxy-hemoglobin decreases at longer wavelengths. Without the capacity to measure the hemoglobin content in the sampled tissue, reduction in blood volume may be incorrectly interpreted as a relative increase in oxygenated hemoglobin. Thus commercial, continuous-wave oximeters may over-estimate ScO_2 in low volume states such as DHCA, as reported here, and their clinical use during these cases should be limited.

A limitation in the present study was the high prevalence of poor data quality due to the optical probe being dislodged after placement. Improvements to the interface of the optical probe (*e.g.*, addition of an adhesive surface) are currently underway, and a study with more subjects wherein this issue is addressed is needed. Additionally cerebral oxygen metabolism is only approximately quantified in this study during DHCA, due to the failure of a simple steady state approximation during the circulatory arrest process. However, since cerebral blood flow is negligible in circulatory arrest, it is likely that oxygen extraction fraction is a good indication for oxygen utilization and thus metabolism in this state.

Conclusion

Cerebral oxygen saturation decreases during DHCA, and the magnitude of this decrease predicts incidence of new postoperative WMI. This knowledge of persistent cerebral oxygen extraction under deep hypothermic conditions may provide useful information for decisions about whether to employ DHCA, and if so for how long, versus a continuous cerebral perfusion strategy. Individual monitoring of cerebral oxygen saturation during DHCA is desirable too, based on the heterogeneity of trends we have observed. Commercial NIRS oximeters may fail to accurately capture this desaturation during DHCA. Ultimately, individual differences in continued oxygen extraction need to be better understood as persistent oxygen extraction during DHCA may lead to increased risk for white matter

injury for some individuals with longer times of DHCA. These pilot results and their clinical implications merit further investigation.

Supplementary Material

Refer to Web version on PubMed Central for supplementary material.

Acknowledgements

We acknowledge invaluable assistance from Timothy W. Boorady, Mahima Devarajan, Kobina Mensah-Brown, Wesley Baker, Richard Melchior, Molly Dreher, the staff of the cardiac operating rooms and intensive care unit at the Children's Hospital of Philadelphia, and most importantly the patients and their families.

Funding Sources:

This study was supported by the NIH Grant Nos. NS-072338, NS-060653, HL-007954, HL-007915, P41-EB015893, the Thrasher Research Foundation, and the June and Steve Wolfson Family foundation.

Appendix

To enable the measurement of absolute concentrations of deoxy-hemoglobin ([Hb]) and oxy-hemoglobin ([HbO₂]), FD-DOS data were also collected on a solid phantom with known optical properties prior to placing the probe on the patient's forehead. The phantom data facilitated calculation of the coupling coefficients between optical fibers and tissue.³³

FD-DOS data were analyzed using the semi-infinite solution to the photon diffusion equation for a homogeneous medium. The phase and AC amplitude (AC) of the detected light are used to quantify the optical properties of the tissue. Specifically, the slope of phase versus source-detector separation (r) and the slope of $\ln(AC \times r^2)$ versus r were determined and used to compute tissue absorption and scattering coefficients: $\mu_a(\lambda)$ and $\mu_s'(\lambda)$, respectively.²⁰ Data were discarded if these linear fits had a Pearson $R^2 < 0.975$. In the near infrared, tissue absorption in brain tissue is primarily a result of [HbO₂], [Hb], and water:

$$\mu_a(\lambda) = \epsilon_{HbO_2}(\lambda) \times [HbO_2] + \epsilon_{Hb}(\lambda) \times [Hb] + 0.75 \times \mu_{a, H_2O}(\lambda) \quad (3)$$

Here, $\epsilon_{HbO_2}(\lambda)$ and $\epsilon_{Hb}(\lambda)$ are the known wavelength extinction coefficients of HbO₂ and Hb, respectively, $\mu_{a, H_2O}(\lambda)$ is the absorption of pure water at wavelength, and we have assumed that brain tissue volume is approximately 75% water. We reconstructed average [Hb] and [HbO₂] from tissue absorption measurements at 2 wavelengths (688 nm and 826 nm) via the system of 2 equations generated by Eq. 1. From [Hb] and [HbO₂], we derived ScO₂: $ScO_2 = [HbO_2]/([Hb] + [HbO_2]) \times 100\%$. Oxygen extraction fraction (OEF) can be calculated from ScO₂ and arterial oxygenation (SaO₂) from the following equation:

$$OEF = \frac{SaO_2 - SvO_2}{SaO_2} = \frac{SaO_2 - ScO_2}{\gamma \times SaO_2} \quad (4)$$

where γ is the percentage of blood in the venous compartment and is assumed to be 75%.

For DCS, each measured intensity autocorrelation function was fit to obtain a CBF_i using the semi-infinite solution to the correlation diffusion equation for a homogenous medium. The tissue optical properties μ_a and μ_s' at the DCS wavelength (785 nm) are required inputs to the fit for CBF_i . Although we only measured these coefficients at 688 nm and 826 nm, we were able to derive μ_a (785 nm) using measured [Hb] and [HbO₂] along with the known Hb and HbO₂ extinction coefficients at 785 nm using Eq. 1. To derive μ_s' (785 nm), we assumed a power-law wavelength dependence for $\mu_s'(\lambda)$ (ie, $\mu_s'(\lambda) = A \lambda^{-b}$), where A and b depend on the size and number of scatters.³⁴

The data acquired from FD-DOS and DCS—namely, ScO₂ and CBF_i —were combined to give a index of cerebral metabolic rate of oxygen ($CMRO_{2,i}$) using Fick's law:

$$CMRO_{2,i} = OEF \times CBF_i \times CaO_2 \quad (5)$$

where CaO_2 is the arterial oxygen content which can be calculated using the formula:

$$CaO_2 = 1.39 \times SaO_2 \times [Hgb] + 0.003 \times PaO_2 \quad (6)$$

Here, 1.39 is the amount of oxygen in milliliters that a fully saturated gram of hemoglobin can carry; PaO_2 is the partial pressure of oxygen in arterial blood, which is measured from an arterial blood gas and has units of mmHg; SaO_2 is the arterial oxygen saturation; and $[Hgb]$ is the hemoglobin concentration of arterial blood in units of grams per deciliter. CaO_2 has units of milliliters of O₂ per deciliter of blood. (5 yields $CMRO_2$ in units of milliliters of O₂ per minute per 100 g of tissue.

Abbreviations and Acronyms

CBF_i	cerebral blood flow index
CBF	cerebral blood flow
CBV	cerebral blood volume
CHD	congenital heart disease/defect
CICU	cardiac intensive care unit
CHOP	The Children's Hospital of Philadelphia
CMRO₂	cerebral metabolic rate of oxygen
CW-NIRS	continuous-wave near infrared spectroscopy
DCS	diffuse correlation spectroscopy
FD-DOS	frequency-domain diffuse optical spectroscopy
FD-NIRS	frequency-domain near infrared spectroscopy
Hb	deoxyhemoglobin, measured with DOS
HbO₂	oxyhemoglobin, measured with DOS

Hct	hematocrit, measured from blood gas
Hgb	hemoglobin, measured from blood gas
HLHS	hypoplastic left heart syndrome
IQR	interquartile range
OEF	cerebral oxygen extraction fraction
SpO₂	peripheral capillary oxygen saturation
ScO₂	cerebral tissue oxygen saturation
WMI	white matter injury

References

- Hoffman JIE & Kaplan S The incidence of congenital heart disease. *J. Am. Coll. Cardiol* 39, 1890–1900 (2002). [PubMed: 12084585]
- Mahle WT et al. An MRI study on neurological injury before and after congenital heart surgery. *Circulation* 106, 109–114 (2002).
- Guo T et al. White matter injury in term neonates with congenital heart diseases: Topology & comparison with preterm newborns. *Neuroimage* 185, 742–749 (2019). [PubMed: 29890324]
- Tusor N et al. Punctate white matter lesions associated with altered brain development and adverse motor outcome in preterm infants. *Sci. Rep* 7, 13250 (2017). [PubMed: 29038505]
- Bellinger DC et al. Adolescents With d-Transposition of the Great Arteries Corrected With the Atrial Switch Procedure. *Pediatr. Cardiol* 124, 1361–1369 (2011).
- Wernovsky G, Shillingford AJ & Gaynor JW Central nervous system outcomes in children with complex congenital heart disease. *Curr. Opin. Cardiol* 20, 94–99 (2005). [PubMed: 15711194]
- Aylward GP Neurodevelopmental Outcomes of Infants Born Prematurely. *J. Dev. Behav. Pediatr* 35, 394–407 (2014). [PubMed: 25007063]
- Johnson S Cognitive and behavioral outcomes following very preterm birth. *Semin Fetal Neonatal Med* 12, 363–373 (2007).
- Andropoulos DB et al. Brain immaturity is associated with brain injury before and after neonatal cardiac surgery with high-flow bypass and cerebral oxygenation monitoring. *J. Thorac. Cardiovasc. Surg* 139, 543–556 (2010). [PubMed: 19909994]
- Beca J et al. New white matter injury after infant heart surgery is associated with diagnostic group and use of circulatory arrest. *Circulation* 127, 917–979 (2013).
- Lynch JM et al. Time-to-Surgery and Pre-operative Cerebral Hemodynamics Predict Post-operative White Matter Injury in Neonates with Hypoplastic Left Heart Syndrome. *J. Thorac. Cardiovasc. Surg* 148, 2181–2188 (2014). [PubMed: 25109755]
- Petit CJ et al. Preoperative brain injury in transposition of the great arteries is associated with oxygenation and time to surgery, not balloon atrial septostomy. *Circulation* 119, 709–716 (2009). [PubMed: 19171858]
- Kinney HC, Panigrahy A, Newburger JW, Jonas RA & Sleeper LA Hypoxic-schemic brain injury in infants with congenital heart disease dying after cardiac surgery. *Acta Neuropathol.* 110, 563–578 (2005). [PubMed: 16244891]
- Algra SO et al. Neurological Injury after Neonatal Cardiac Surgery: A Randomized Controlled Trial of Two Perfusion Techniques. *Circulation* (2013).
- Durduran T, Choe R, Baker WB & Yodh AG Diffuse optics for tissue monitoring and tomography. *Reports Prog. Phys* 73, (2010).
- Jain V et al. Cerebral oxygen metabolism in neonates with congenital heart disease quantified by MRI and optics. *J. Cereb. Blood Flow Metab* 34, (2014). [PubMed: 24045400]

17. Busch DR et al. Continuous cerebral hemodynamic measurement during deep hypothermic circulatory arrest. *Biomed. Opt. Express* 7, 3461 (2016). [PubMed: 27699112]
18. Buckley EM et al. Validation of diffuse correlation spectroscopic measurement of cerebral blood flow using phase-encoded velocity mapping magnetic resonance imaging. *J. Biomed. Opt* 17, (2012).
19. Buckley EM et al. Early Post-Operative Changes in Cerebral Oxygen Metabolism Following Neonatal Cardiac Surgery: Effects of Surgical Duration. *J. Thorac. Cardiovasc. Surg* 145, 196–205 (2012). [PubMed: 23111021]
20. Durduran T et al. Optical measurement of cerebral hemodynamics and oxygen metabolism in neonates with congenital heart defects. *J. Biomed. Opt* 15, 37004 (2010).
21. Wyatt JS, Delpy DT, Cope M, Wray S & Reynolds EOR Quantification of cerebral oxygenation and haemodynamics in sick newborn infants by near infrared spectrophotometry. *Lancet* 328, 1063–1066 (1986).
22. Boas DA & Yodh AG Spatially varying dynamical properties of turbid media probed with diffusing temporal light correlation. *J. Opt. Soc. Am. A* 14, 192–215 (1997).
23. Pine DJ, Weitz DA, Chaikin PM & Herbolzheimer E Diffusing wave spectroscopy. *Phys. Rev. Lett* 60, 1134–1137 (1988). [PubMed: 10037950]
24. Buckley EM et al. Cerebral hemodynamics in preterm infants during positional intervention measured with diffuse correlation spectroscopy and transcranial Doppler ultrasound. *Opt. Express* 17, 12571–12581 (2009). [PubMed: 19654660]
25. He L et al. Noninvasive continuous optical monitoring of absolute cerebral blood flow in critically ill adults. *Neurophotonics* 5, 45006 (2018).
26. Milej D et al. Quantification of cerebral blood flow in adults by contrast-enhanced near-infrared spectroscopy: Validation against MRI. *J. Cereb. Blood Flow Metab* Sep 9:2716, (2019).
27. Roche-Labarbe N et al. Noninvasive optical measures of CBV, StO₂, CBF index, and rCMRO₂ in human premature neonates' brain in the first six weeks of life. *Hum. Brain Mapp* 31, 341–352 (2010). [PubMed: 19650140]
28. Ko TS et al. Non-invasive optical neuromonitoring of the temperature-dependence of cerebral oxygen metabolism during deep hypothermic cardiopulmonary bypass in neonatal swine. *J. Cereb. Blood Flow Metab* 40, (2020).
29. Mavroudis CD et al. Electroencephalographic Response to Deep Hypothermic Circulatory Arrest in Neonatal Swine and Humans. *Ann. Thorac. Surg* 106, 1841–1846 (2018). [PubMed: 30071237]
30. Greeley WJ et al. The effect of hypothermic cardiopulmonary bypass and total circulatory arrest on cerebral metabolism in neonates, infants, and children. *J. Thorac. Cardiovasc. Surg* 101, 783–794 (1991). [PubMed: 2023435]
31. Shin'oka T, Nollert G, Shum-Tim D, Du Plessis A & Jonas RA Utility of near-infrared spectroscopic measurements during deep hypothermic circulatory arrest. *Ann. Thorac. Surg* 69, 578–583 (2000). [PubMed: 10735702]
32. Lynch JM et al. Pre-Operative Cerebral Hemodynamics from Birth to Surgery in Neonates with Critical Congenital Heart Disease. *J. Thorac. Cardiovasc. Surg* 156, 1657–1664 (2018). [PubMed: 29859676]
33. Hueber DM et al. Non-invasive and quantitative near-infrared haemoglobin spectrometry in the piglet brain during hypoxic stress, using a frequency-domain multidistance instrument. *Phys. Med. Biol* 46, (2000).
34. Mourant JR et al. Mechanisms of light scattering from biological cells relevant to noninvasive optical-tissue diagnostics. *Appl. Opt* 37, 3586–3593 (1998). [PubMed: 18273328]

Central Message

Cerebral oxygen saturation decreases during deep hypothermic circulatory arrest, and the extent of this decrease in oxygenation is associated with an increased risk of postoperative brain injury.

Author Manuscript

Author Manuscript

Author Manuscript

Author Manuscript

Perspective Statement

A main focus of research on complex congenital heart disease is on modifiable risk factors for brain injury. Investigations into the association between perfusion strategies and brain injury have had conflicting results. We observe that cerebral oxygen saturation continues to decrease during DHCA and that greater decreases in oxygenation are associated with an increased risk for postoperative brain injury.

Author Manuscript

Author Manuscript

Author Manuscript

Author Manuscript

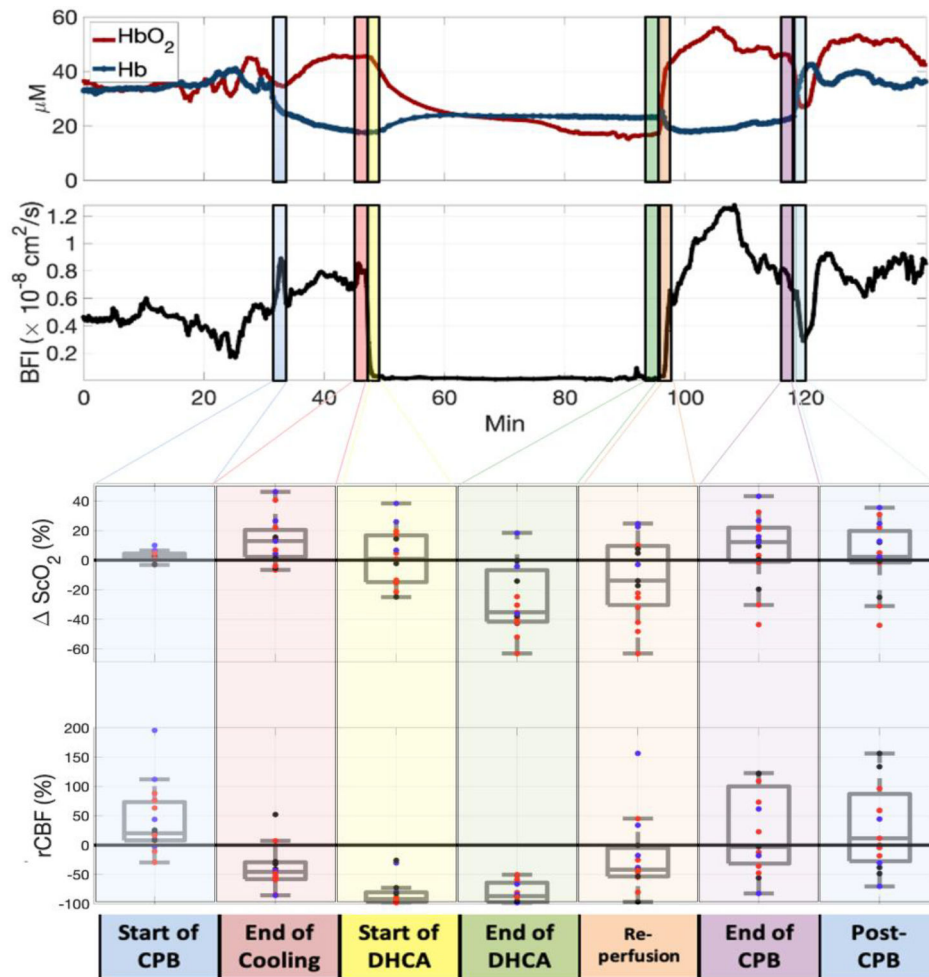


Figure 1.

The top two panels demonstrate a sample time-series of continuous optical data from one study subject throughout surgery: concentration of oxy- (red) and deoxy- (blue) hemoglobin (a) and cerebral blood flow index (CBFi) (b). Vertical lines indicate the start and stop times of cardiopulmonary bypass (CPB) and deep hypothermic circulatory arrest (DHCA), and the colored rectangles correspond to points of time in the boxplots below. The bottom two panels are boxplots demonstrating changes in cerebral tissue oxygen saturation (ScO₂) (c) and relative cerebral blood flow (CBF) (d) for all 15 subjects at 7 different time points: (1) start of CPB and cooling, (2) end of cooling, (3) start of DHCA, (4) end of DHCA, (5) reperfusion/rewarming, (6) end of CPB, (7) after CPB. Each time point represents an average over 2 minutes. Changes are compared to a 2-minute baseline period immediately prior to the start of CPB. The color of the individual data points represents if the subject had new post-operative white matter injury (WMI) (red) or did not have new post-operative injury (blue), with black representing subjects for which MRI was not performed.

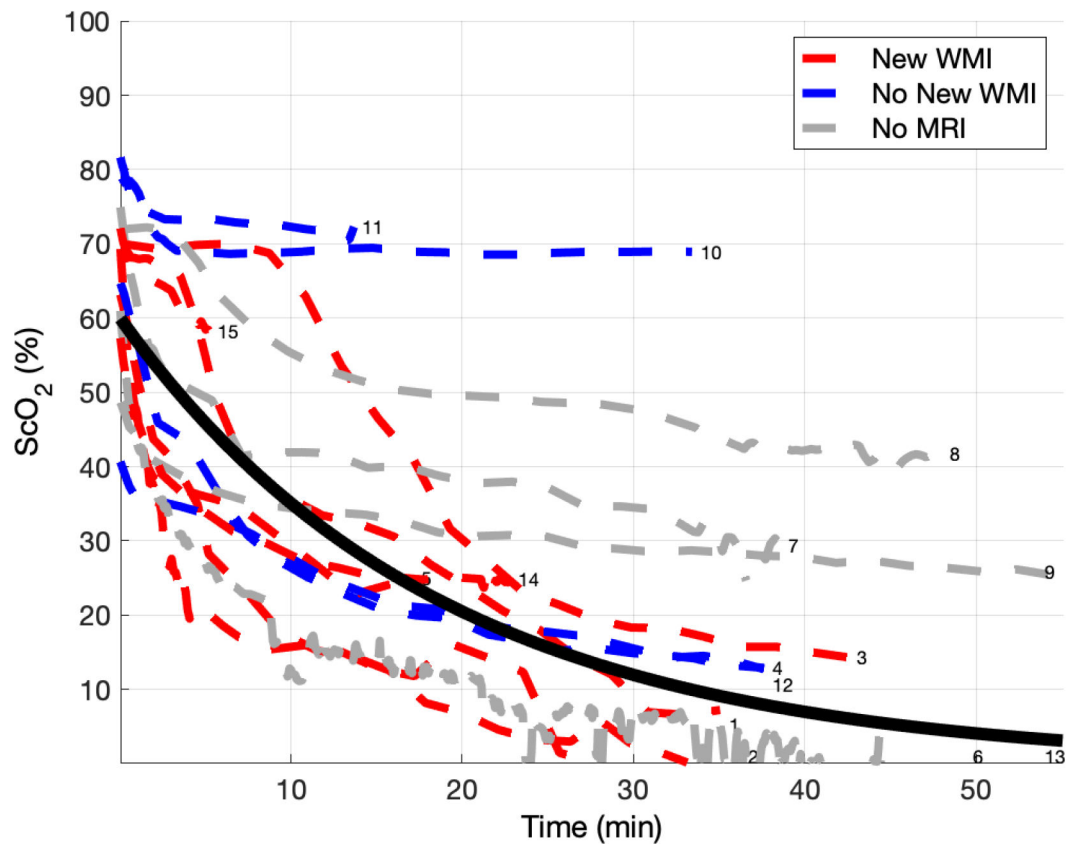


Figure 2. Cerebral tissue oxygen saturation (ScO_2) during deep hypothermic circulatory arrest (DHCA) for all 15 subjects. Time axis represents time on circulatory arrest. Each dotted line represents an individual subject. The color of each dotted line represents whether new postoperative white matter injury (WMI) was (red) or was not (blue) present, with a gray dotted line representing subjects for which a post-operative MRI was not performed (N=4). The solid black line is the line of best fit when fitting the data to an exponential decay. Curves are numbered with subject identifier (see Table 3).

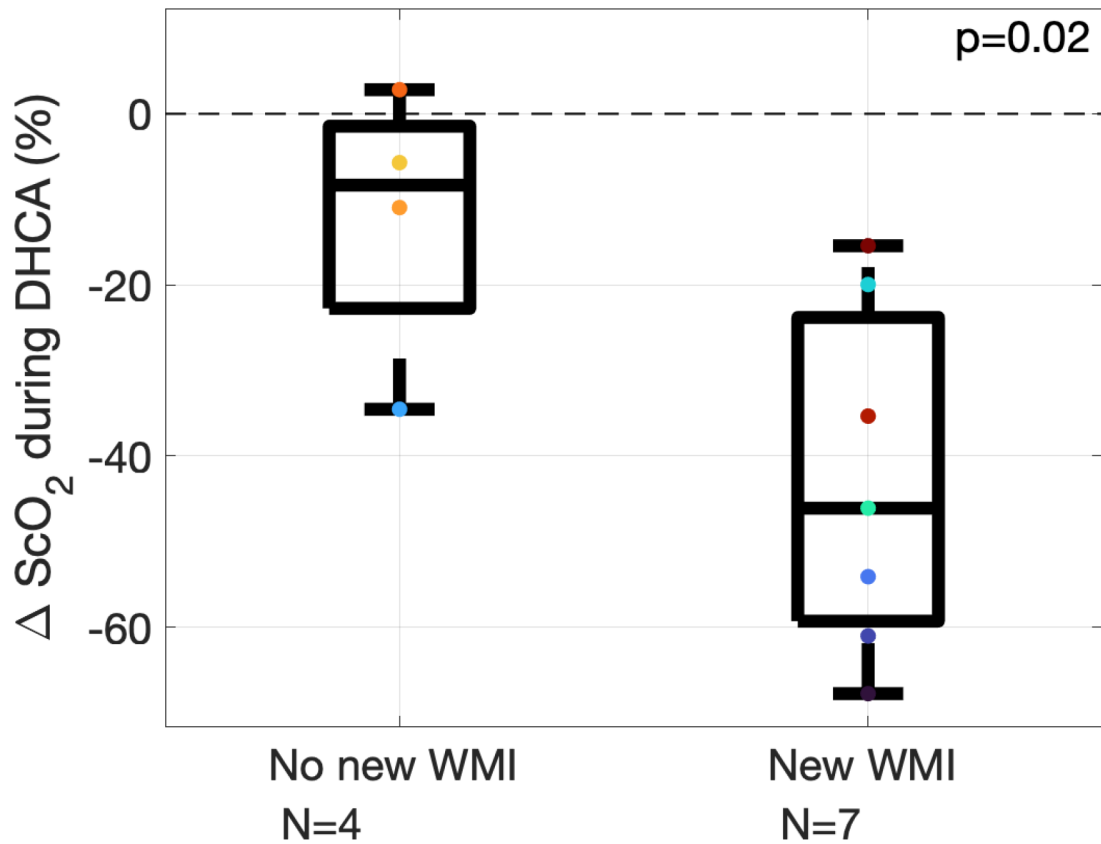


Figure 3.

Change in cerebral tissue oxygen saturation (ScO_2) during deep hypothermic circulatory arrest (DHCA) for subjects who did not have new white matter injury (WMI) on post-operative MRI (left, n=4) and subjects that did (right, n=7). On each box, the central line indicates the median, and the bottom and top edges of the box indicate the 25th and 75th percentiles, respectively. The whiskers extend to the most extreme data points not considered outliers. Each individual subject's data is represented by colored marks.

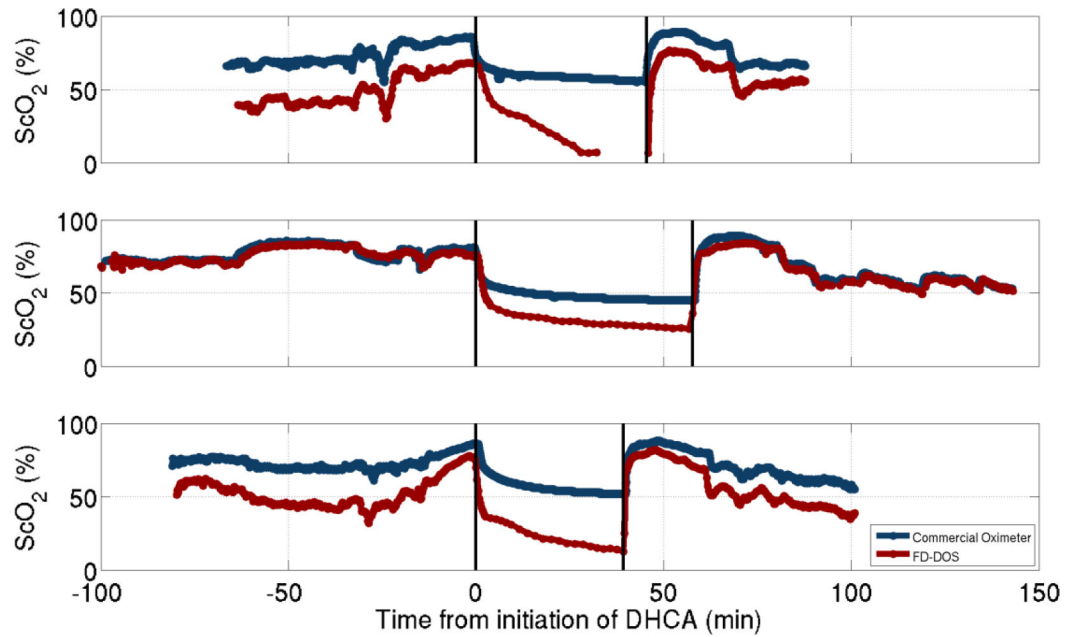


Figure 4.

Comparison of frequency domain diffuse optical spectroscopy (FD-DOS) (red) and a continuous-wave commercial oximeter (blue) over the course of the surgery for three subjects. Vertical lines indicate period of deep hypothermic circulatory arrest.

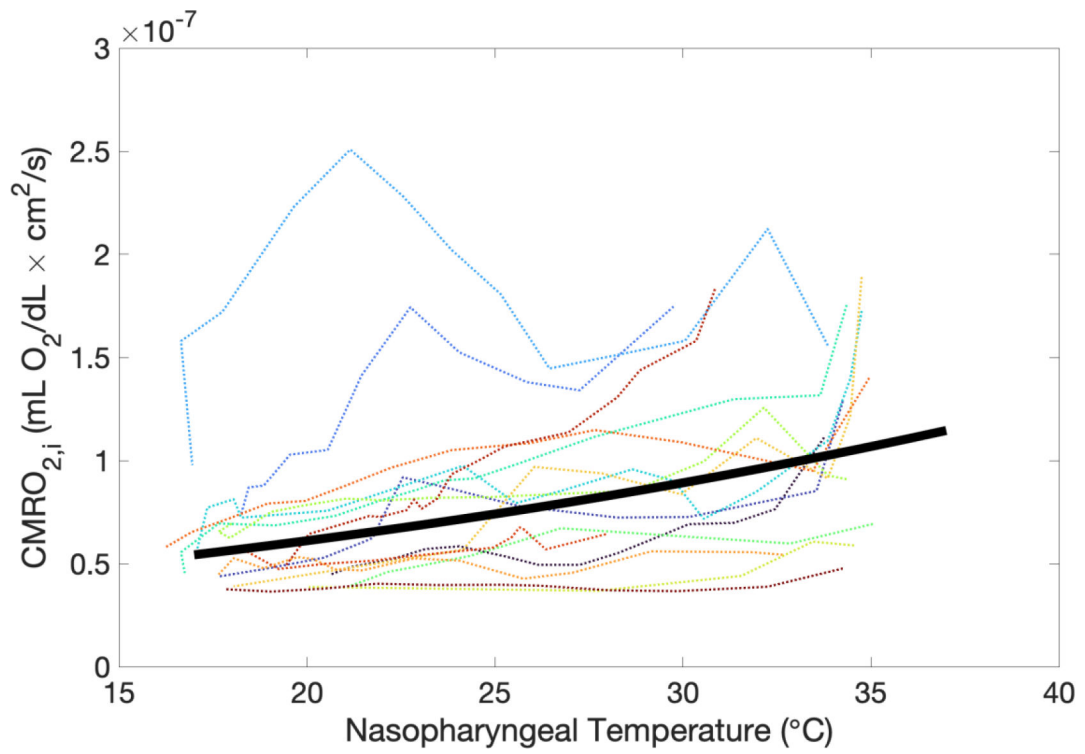


Figure 5:
 Index of cerebral metabolic rate of oxygen ($CMRO_{2,i}$) versus nasopharyngeal temperature for all 15 subjects (dotted line). The solid line is the result of fitting the data to the form $\ln(CMRO_{2,i}) = \frac{E_a}{R} \left(\frac{1}{T} \right) + \ln(A)$ (see Methods and Results).

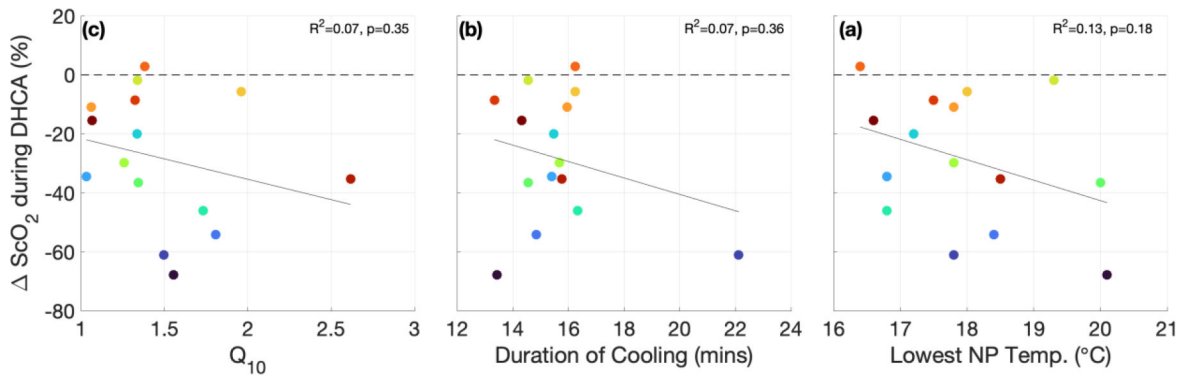


Figure 6.

The lowest nasopharyngeal temperature achieved during cooling (a), duration of cooling prior to deep hypothermic circulatory arrest (DHCA) (b), and cerebral metabolic rate of oxygen temperature coefficient, Q_{10} , (c) versus change in cerebral tissue oxygen saturation during DHCA.

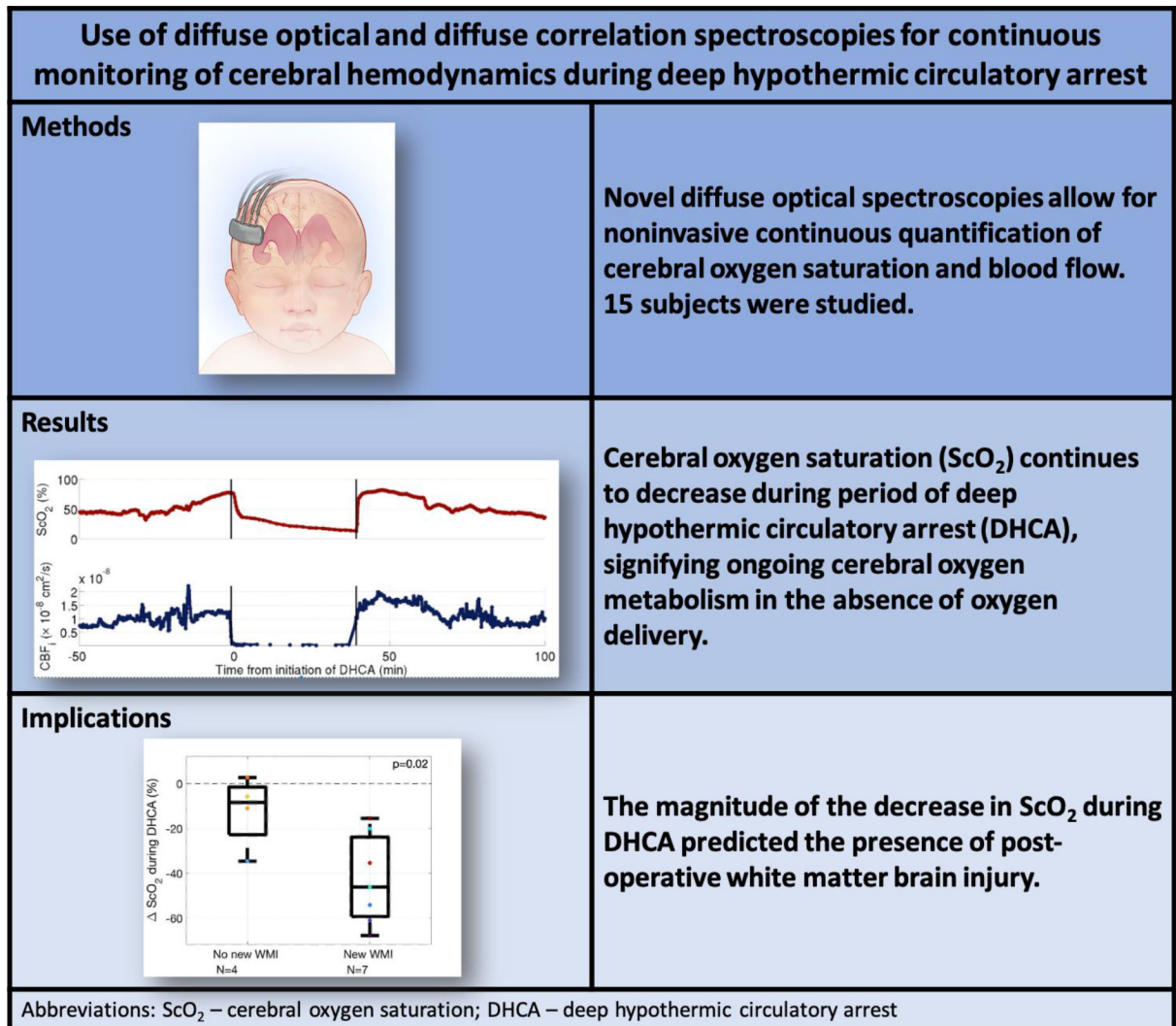
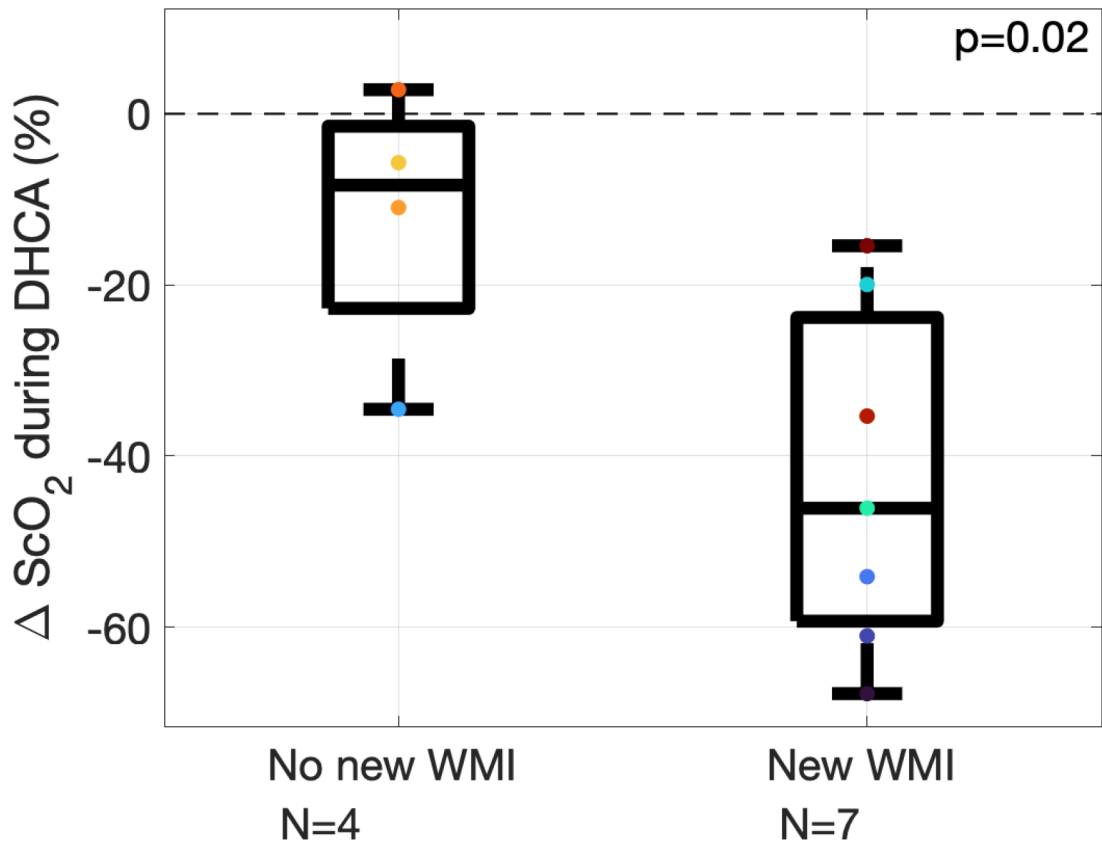


Figure 7.

Frequency-domain diffuse optical spectroscopy and diffuse correlation spectroscopy allow for noninvasive, continuous quantification of cerebral oxygen saturation (ScO_2) and blood flow (CBF_i). Using these devices, we observed a decrease in ScO_2 during deep hypothermic circulatory arrest (DHCA). The magnitude of the decrease in ScO_2 during DHCA was predictive of post-operative white matter brain injury.



Central Picture Legend.
Greater decreases in ScO₂ during DHCA are associated with post-operative brain injury.

Author Manuscript

Author Manuscript

Author Manuscript

Author Manuscript

Table 1

Patient demographics and operative parameters. Normally distributed data are reported as mean standard deviation and data that are not normally distributed are reported as median (interquartile range).

<i>Demographics</i>	
Female, n (%)	6 (40)
Time-to-surgery, day	3.7 ± 1.4
Gest. age, wk	38.6 ± 0.7
Birth weight, kg	3.3 ± 0.5
Head circumference, cm	34.2 ± 1.1
<i>Operative Parameters</i>	
Duration of cooling, min	15.5 (1.6)
Duration of rewarming, min	22.7 (10.4)
Rate of cooling, °C/min	-1.1 ± 0.1
Lowest NP temperature, °C	17.9 ± 1.2
DHCA duration, min	40 (12.8)
Total support time, min	85 (21)

Author Manuscript

Author Manuscript

Author Manuscript

Author Manuscript

Table 2

Presence and volume of white matter injury (MRI) on pre- and post-operative magnetic resonance imaging. Continuous data is reported as median (interquartile range).

<i>MRI Measured Parameters</i>	
Presence of pre-operative WMI, n(%)	3 (20)
Volume of pre-operative WMI, mm ³	6.3 (3.9)
Presence of new post-operative WMI, n(%)	8 (73)
Volume of new post-operative WMI, mm ³	30.3 (219.3)

Author Manuscript

Author Manuscript

Author Manuscript

Author Manuscript

Table 3:

Individual patient characteristics

<i>Subject</i>	<i>Age at surgery (days)</i>	<i>Presence of preoperative WMI</i>	<i>Presence of new or worse postoperative WMI</i>	<i>Number of CPB runs</i>	<i>Number of DHCA runs</i>
1	4	No	Yes	1	1
2	3	No	Yes	2	1
3	2	Yes	Yes	1	1
4	5	Yes	No	1	1
5	3	No	Yes	1	1
6	6	No	Yes	1	1
7	2	MRI not performed	MRI not performed	1	1
8	5	No	MRI not performed	1	1
9	1	No	MRI not performed	1	1
10	2	No	No	1	1
11	4	No	No	1	1
12	4	No	No	1	1
13	4	No	MRI not performed	1	1
14	5	Yes	Yes	2	2
15	5	No	Yes	1	1

WMI = White Matter Injury; CPB = Cardiopulmonary Bypass; DHCA = deep hypothermic circulatory arrest